Hot-phonon lifetime in $Al_{0.23}Ga_{0.77}N$/GaN channels

2014 Semicond. Sci. Technol. 29 045018

(http://iopscience.iop.org/0268-1242/29/4/045018)

IOP Publishing Semiconductor Science and Technology
Semicond. Sci. Technol. **29** (2014) 045018 (7pp) doi:10.1088/0268-1242/29/4/045018

Hot-phonon lifetime in $Al_{0.23}Ga_{0.77}N$/GaN channels

J Liberis[1], M Ramonas[1], E Šermukšnis[1], P Sakalas[1], N Szabo[2], M Schuster[2], A Wachowiak[2] and A Matulionis[1]

[1] Fluctuation Research Laboratory, Semiconductor Physics Institute, Centre for Physical Sciences and Technology, 01108 Vilnius, Lithuania
[2] NaMLab gGmbH (Nano-electronic Materials Laboratory), D-01187 Dresden, Germany

E-mail: jlbrs@pfi.lt

Received 29 November 2013, revised 6 February 2014
Accepted for publication 10 February 2014
Published 26 February 2014

Abstract

Hot-phonon effects on hot-electron noise and transport are investigated in nominally undoped two-dimensional $Al_{0.23}Ga_{0.77}N$/GaN channel with electron density of 7.4×10^{12} cm^{-2}. The electrons are subjected to electric field applied in the channel plane. The dependence of noise temperature on supplied electric power yields hot-phonon lifetime of (370 ± 100) fs at low levels of power (<1 nW/electron). Monte Carlo simulation of hot-electron drift velocity with the same lifetime value as a model parameter confirms the experimental findings. The lifetime decreases as the supplied power increases until the values below 50 fs are deduced at high level of power (>10 nW/electron). These values are substantially lower than the plasmon-free lifetime, and the experimental data are interpreted in terms of plasmon-assisted conversion of hot phonons into acoustic phonons and to other vibration modes.

Keywords: HEMTs, electron gas, hot electrons, hot phonons, fluctuations

(Some figures may appear in colour only in the online journal)

1. Introduction

Wide band-gap semiconductor devices suit power switching applications if they combine high current in on-state with high breakdown voltage in off-state. These requirements are met by a channel with a quasi-two-dimensional electron gas (2DEG) confined in a nominally undoped GaN layer of a nitride heterostructure grown on an electrically non-conductive substrate [1, 2]. One unsolved problem is heat dissipation aggravated by accumulation of non-equilibrium longitudinal optical (LO) phonons, often named—hot phonons [3]. While the traditional approach focuses on heat drain through the non-conductive layers, special attention should be paid to the so-called LO-mode heat when its conversion into other heat modes constitutes a bottleneck for heat dissipation [4].

Because of strong Fröhlich interaction of electrons with LO phonons (e–LO scattering) in GaN, the heat generated by the current is shared by the hot electrons and the hot phonons—the hot subsystem forms [5]. The shared heat stays in the 2DEG channel until the LO-mode heat is converted into the heat modes able to propagate across the electrically non-conductive layers towards the remote heat sink. The bottleneck forms if the hot-phonon conversion is slow. The associated hot-phonon lifetime is several picoseconds in GaN unless electron density effects are involved [6, 7]. Hot phonons introduce additional scattering for the drifting electrons and hence, a longer lifetime causes lower drift velocity [5]. As a result, the hot-phonon lifetime is important for the on-state current. Moreover, hot phonons facilitate defect formation when the current flows [8, 9]. The hot-phonon effects are weaker when the lifetime is shorter.

Plasmons are known to reduce the hot-phonon lifetime, since they enable an alternative relaxation path for hot phonons [7–11]. The relaxation becomes faster as the plasma frequency approaches that of the LO-phonon: the lifetime acquires the shortest value at some resonance 2DEG density of ~6.5×10^{12} cm^{-2} and ~2.7×10^{12} cm^{-2} in nitride and arsenide 2DEG channels, respectively [11, 12].

The plasma frequency decreases as the 2DEG occupies more volume at elevated hot-electron temperatures when the electrons are heated with the longitudinal electric field

[13]. This opens the opportunity for tuning the channel into the resonance if the initial 2DEG density exceeds the resonance one. The related tunable ultrafast conversion of hot phonons has been reported for the channels embedded in InAlN/AlN/GaN [14] and InAlN/AlN/AlGaN/GaN structures [15].

The plasmon-assisted resonance has also been resolved in heterostructure field-effect transistors (HFETs) [16, 17]. The resonance 2DEG density is reached in the channel underneath the gate when the negative bias is applied to the gate terminal for the optimal frequency performance. The same bias supports slowest degradation of the channel [8, 9]. Thus, the plasmon-assisted conversion of hot phonons is important for cut-off frequency and reliability of HFETs. For power electronics in the lower frequency range (100 kHz–1 MHz), a negative gate bias for HFETs would cause a lower 2DEG density in on-state and therefore a trade-off between desired high 2DEG density and short hot-phonon lifetime is expected for optimum operation of largest current drive.

Our goal is to estimate the hot-phonon lifetime in the 2DEG channel of $Al_{0.23}Ga_{0.77}N$/GaN structure through investigation of hot-electron transport and fluctuations. A pulsed experimental technique, based on hot-electron noise, is used for demonstration of power-tunable plasmon-assisted hot-phonon conversion.

2. Samples and techniques

The investigated $Al_{0.23}Ga_{0.77}N$/GaN structures were grown at the Ferdinand Braun Institut, Berlin by metalorganic compound vapour phase epitaxy on c-sapphire substrate. The growth was initiated with a 20 nm low-temperature GaN layer, followed with a 2 μm partially Fe-doped GaN buffer layer topped with a nominally undoped GaN layer of nanometric thickness, covered with a 17 nm $Al_{0.23}Ga_{0.77}N$ nominally undoped barrier layer and capped with a 3 nm Si-doped GaN cap layer.

The energy diagram of the $Al_{0.23}Ga_{0.77}N$/GaN structure is obtained through self-consistent solution of coupled one-dimensional Poisson and Schrödinger equations in the way described elsewhere [18]. The polarization and piezoelectric charges ($\sigma/e = 1.02 \times 10^{13}$ cm^{-2}) formed the 2DEG channel with electron density of 7.4×10^{12} cm^{-2} in the undoped GaN at the heterojunction with the $Al_{0.23}Ga_{0.77}N$. Solid line in figure 1 illustrates dependence of the conduction band edge energy on position for the investigated structure. The electron gas is degenerate at equilibrium: the Fermi level (dash-dot line) is located inside the lowest subband below the second subband. The electron wave functions for the three lowest subbands are shown as black broken lines in the inset of figure 1. The main peak of each wave function is located in the GaN layer, but the tails penetrate into the barrier layer. As expected, the penetration is more pronounced for the upper subbands. In particular, the secondary extreme of the third subband is located inside the $Al_{0.23}Ga_{0.77}N$ layer.

The transmission line method (TLM) patterns with 100 μm-wide coplanar electrodes are defined through standard photolithography and lift-off procedure. In order to obtain

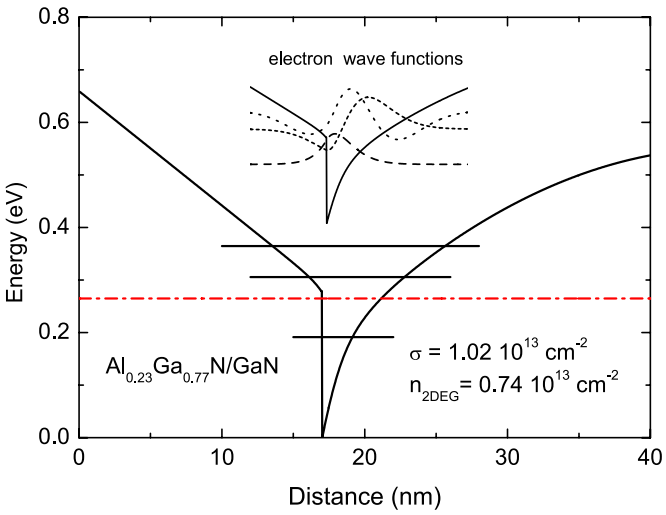

Figure 1. Dependence on distance perpendicular to channel plane of conduction band edge energy (solid line). Fermi energy is represented by dashed-dotted line, and electron energy levels for three lowest subbands are represented by horizontal bars. Envelope wave functions for three lowest subbands are given in the inset.

a low resistive, ohmic contact to the buried 2DEG channel, a metal stack of Ti/Al/Ni/Au (35/200/40/100 nm) was deposited and annealed at 800 °C for 30 s in nitrogen ambient. Some samples were passivated by atomic layer deposition of 10 nm AlOx. The dependence of the channel resistance on its length is approximated by the: $(7.0 + 4.7L)\Omega$ and $(10.05 + 7.4L)\Omega$, correspondingly, for the samples A (passivated) and B (unpassivated) where channel length L is measured in micrometres. Extraction of channel resistivity and contact resistance from linear fitting of the TLM values gives 470 Ω/□ and 0.7 Ω×mm and 740 Ω/□ and 1.0 Ω×mm for the passivated and unpassivated sample, respectively. The area specific contact resistivity is similar for both samples, $\sim$1.0–1.3 $\times 10^{-5}$ Ω×cm^2. The difference in channel resistivity is caused by different mobility, as obtained from independent magnetoresistance measurements. The deduced electron density is comparable in both samples and agrees well with the calculated value. Table 1 summarizes the respective values of the two samples.

Pulsed technique is used to investigate hot-electron and hot-phonon effects. Because of almost elastic electron–acoustic-phonon scattering and strong Fröhlich (e–LO) interaction, the hot electrons share the heat predominately with the hot phonons. The hot-subsystem is weakly coupled with the thermal bath represented mainly by acoustic phonons which ensure good thermal coupling with the remote heat sink.

For the short duration and small duty cycle pulses one reads

$$T_h - T_0 \gg T_b - T_0, \quad (1)$$

where T_h is the hot-subsystem temperature, T_b is the bath temperature, and T_0 is the heat sink temperature.

Because of high density of electron gas and intense e–LO interaction, the following conditions are satisfied for the hot subsystem confined in a typical GaN-based 2DEG channel [4]:

$$T_h \approx T_e \approx T_{LO}, \quad (2)$$

Table 1. $Al_{0.23}Ga_{0.77}N$/GaN sample data at low electric fields.

Sample	Contact resistance, Ω× mm	Channel resistivity, Ω/□	Channel length, μm	Mobility, cm^2 (V^{-1} s^{-1})	2DEG density, cm^{-2}	Comment
A	0.7	470	6	1790	7.4×10^{12}	Passivated
B	1	740	12	1150	7.3×10^{12}	Unpassivated

where T_e is the hot-electron temperature and T_{LO} is the equivalent hot-phonon temperature. Moreover

$$T_n \approx T_e, \tag{3}$$

where T_n is the hot-electron noise temperature. Therefore, the hot phonons can be investigated through measurements of hot-electron fluctuations. The consumed power per electron is

$$P_c = evE, \tag{4}$$

where e is the elementary charge and v is the electron drift velocity. Since direct heat transfer from the electrons to acoustic phonons is negligible because of almost elastic interaction, the supplied electric power is dissipated mainly through emission of LO phonons by hot electrons followed by the hot-phonon conversion into acoustic phonons. The excess heat leaks out at the rate proportional to the excess occupancy ΔN_{LO} of the hot-phonon states

$$\Delta N_{LO} = N_{LO} - N_b, \tag{5}$$

where N_{LO} is the effective occupancy of the hot-phonon states selected by energy and momentum conservation during the e–LO collisions, and N_b is the background occupancy of the LO-phonon states controlled by the bath temperature T_b. The effective and background occupancies are estimated after the Bose–Einstein formula for the corresponding temperatures, T_{LO} and T_b, obtained through the noise temperature measurements with equations (2) and (3) in mind. When the bath is weakly disturbed, its temperature is close to that of the sink: $T_b \approx T_0$ and $N_b = N(T_0)$. However, this is not the case at elevated hot-electron temperatures.

The effective hot-phonon conversion lifetime can be estimated from the balance of supplied and dissipated power. Supposing that the lifetime is independent of the power, the following expression is used [4]:

$$\tau_{LO} = \frac{\hbar\omega \Delta N_{LO}}{P_c}, \tag{6}$$

where $\hbar\omega$ is the LO-phonon energy (92 meV).

This simplified approach allows one to predict the dependence of hot-electron noise temperature on supplied power. At a given supplied power, an almost linear dependence of the noise temperature on the hot-phonon lifetime is expected. In this way, measurement of the noise temperature and the supplied power can lead to estimation of the lifetime.

The noise temperature is measured at 10 GHz frequency band where flicker and generation–recombination noise sources can be neglected. The experimental setup and the background of the fluctuation technique have been discussed elsewhere [19]. In this paper, the pulsed dc current passes along the gateless channel and heats the electrons. Voltage pulse durations of 2.7 μs and 100 ns are used, at low–moderate electric fields ($E < 4$ kV cm^{-1}) and moderate–high electric fields ($E > 1.5$ kV cm^{-1}), respectively. The bath temperature is estimated through back-extrapolation of the time-dependent (gated) noise temperature measured after the switch-off of the voltage pulse. In particular, an increase in the bath temperature can be ignored at electric fields below 10 kV cm^{-1} for 100 ns voltage pulses. However, the bath temperature reaches ∼450 K at the electric field of ∼30 kV cm^{-1}.

Ensemble Monte Carlo procedure is used to treat electron scattering and hot-phonon effects for the investigated $Al_{0.23}Ga_{0.77}N$/GaN structure. Constant hot-phonon lifetime is assumed, one-valley many-subband spherical parabolic model is used, electron gas degeneracy is taken into account, electron scattering into the upper valleys is ignored, and the bath temperature is kept constant ($T_b = 300$ K). The e–LO scattering rates are evaluated by using the calculated electron wave functions obtained through self-consistent solution of coupled one-dimensional Poisson and Schrödinger equations (figure 1). Impurity scattering and other elastic scattering mechanisms are not included in the simulation; the investigated structures are assumed to be free of intentional doping in the vicinity of the channel and the 2DEG is induced by the polarization charges. Acoustic deformation-potential and piezoelectric scattering (treated as inelastic processes) and LO-phonon polar scattering (cubic approximation) are included. Screening is considered for the piezoelectric and LO-phonon scattering in long-wavelength diagonal approximation derived using the matrix-random phase approach [18]. Material parameters are the same as in [18].

In the ensemble Monte Carlo technique individual e–LO scattering events are simulated. To follow the time evolution of the LO-phonon distribution function the histogram is set over the LO phonon wave vector space. After each e–LO scattering event, the histogram is updated (after emission the phonon number is increased and decreased after absorption). At fixed time steps during the Monte Carlo simulation, the non-equilibrium LO-phonon distribution is calculated from the histogram. To account for the non-equilibrium LO-phonon decay relaxation-time approximation is used. To avoid e–LO scattering rate recalculation after each update of the phonon distribution function the rejection technique is used [18].

Let us evaluate the effective hot-phonon temperature as follows. The Monte Carlo simulation takes into account each event of an electron scattering by an LO phonon. The actual e–LO scattering rate is tabulated. Figure 2 shows the result for the first subband of the investigated $Al_{0.23}Ga_{0.77}N$/GaN heterostructure. The LO-phonon emission brings the electron into the low-energy region unless the selected electron state is occupied. As a consequence, the LO-phonon emission probability is reduced because of the electron gas degeneracy

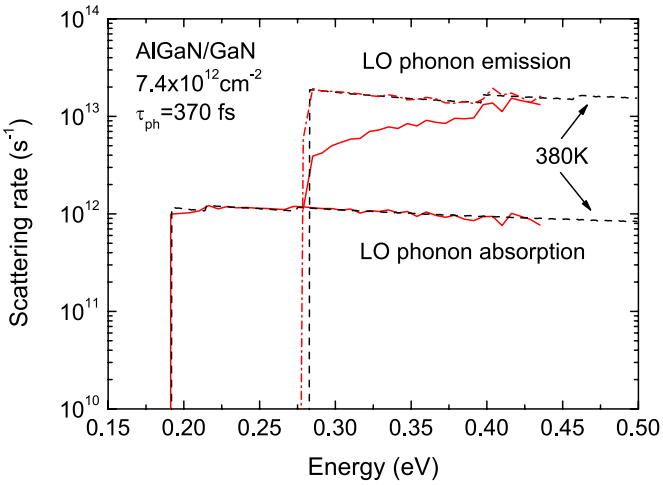

Figure 2. Dependence of e–LO scattering rate on electron energy in the first subband of the investigated $Al_{0.23}Ga_{0.77}N$/GaN heterostructure. Solid lines represent Monte Carlo results for LO-phonon absorption and emission. Dash-dotted line stands for the LO-phonon emission rate obtained through Monte Carlo calculation with electron gas degeneracy effect neglected. Dashed lines represent LO-phonon absorption and emission at zero electric field and 380 K lattice temperature.

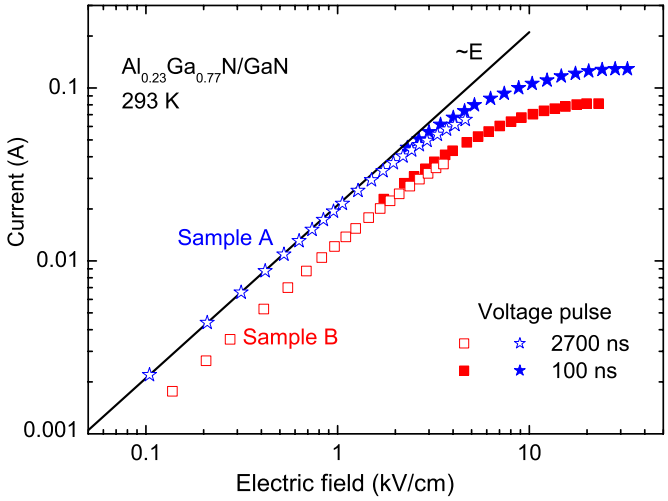

Figure 3. Measured dependence of current on electric field for passivated sample A (stars, channel length 6 μm) and unpassivated sample B (squares, 12 μm). Voltage pulse duration is 2.7 μs (open symbols) and 100 ns (closed symbols). Solid line represents ohmic behaviour for sample A.

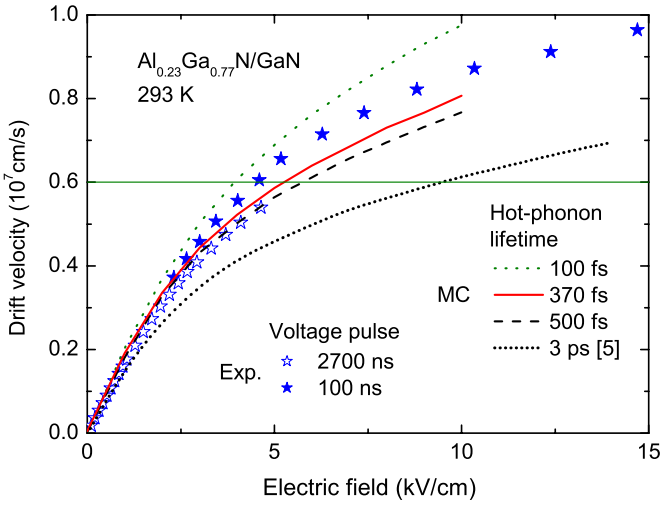

Figure 4. Dependence of drift velocity on electric field. Stars stand for estimated values from experiment for passivated sample A. Lines show Monte Carlo simulation for hot-phonon lifetime: 100 fs (dots), 370 fs (solid line), 500 fs (dashes) and 3 ps (short dots [5]).

(cf solid and dash-dotted lines for the LO-phonon emission in figure 2). The probability of LO-phonon absorption by the electron is proportional to the LO-phonon number. This allows one to evaluate the effective hot-phonon temperature from comparison of the calculated e–LO scattering rate and that caused by the LO phonons distributed according to Bose–Einstein. The electrons experience approximately the same strength of LO scattering at 8 kV cm^{-1} electric field, if the actual hot-phonon distribution function is replaced by the Bose–Einstein distribution with 380 K effective temperature (dashed and solid lines for LO-phonon absorption in figure 2). The Monte Carlo simulation justifies the concept of the effective hot-phonon temperature for the LO-phonons involved in e–LO scattering. The effective electron temperature of 420 K is evaluated from the electron distribution function. According to the simulation, the error makes ∼10%; the condition equation (2) holds within the experimental accuracy. As a result, equation (6) overestimates the lifetime. The overestimation is stronger if the lifetime is shorter.

3. Results

The measured dependence of current on electric field is illustrated in figure 3. A channel length of 6 μm (12 μm) was used for the sample A (B) to minimize the influence of drain contact on the electron power dissipation in the channel. For the unpassivated sample B, the lower electron mobility results to a lower current (squares). An almost linear dependence of current on electric field holds for $E < 2$ kV cm^{-1} (solid line and stars). Non-ohmic behaviour develops at higher electric field. The current at high applied electric field (saturation regime) is sensitive to pulse duration. The dependence on pulse duration points to the heat accumulated in the hot-electron–hot-phonon subsystem and by acoustic phonons as the main reason for the tendency of current to saturation. The deviation from the Ohm law is stronger for 2.7 μs pulses (open stars) as compared with the results for 100 ns pulses (solid stars). This dependence on pulse duration is associated with increase in the bath temperature. For the short voltage pulses, hot electrons and hot phonons are the main origin for non-ohmic behaviour at electric fields in the range below 10 kV cm^{-1}. The bath temperature effects become significant beyond 10 kV cm^{-1}. The electron drift velocity is estimated under assumption of field-independent electron density. The results for sample A are illustrated in figure 4 (symbols). The electron mobility at low electric fields is obtained from the measured magnetoresistance (table 1). The experimental results are compared with Monte Carlo simulation data (lines).

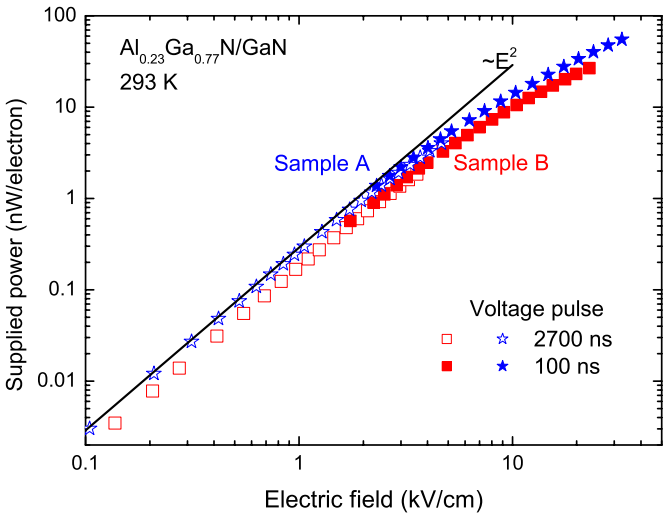

Figure 5. Dependence of supplied power per electron on electric field for passivated sample A (stars) and unpassivated sample B (squares). Voltage pulse duration is 2.7 μs (open symbols) and 100 ns (closed symbols).

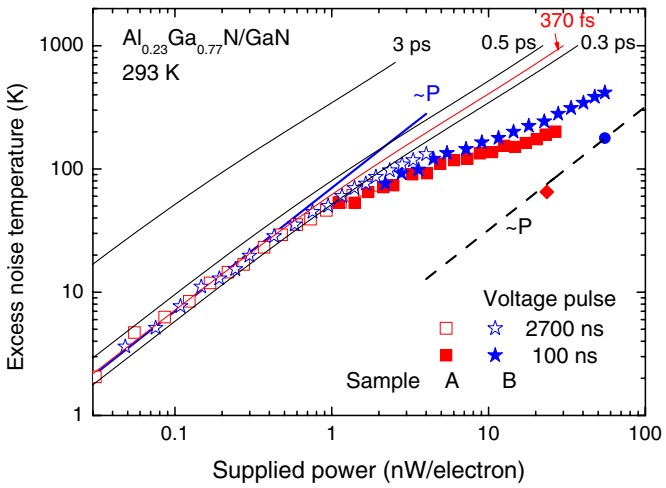

Figure 6. Power-dependent excess noise temperature $T_n - T_0$ for sample A (stars) and sample B (squares). Lines are approximations: blue solid line fits the experimental data at low level of supplied power, thin lines assume power-independent hot-phonon lifetime (3 ps, 0.5 ps, 370 fs and 0.3 ps), dashed line fits the experimental data on power-dependent excess bath temperature $T_b - T_0$ estimated at 55 nW/electron (bullet) and 23 nW/electron (diamond) for samples A and B, respectively.

The simulation is carried out for several input values of hot-phonon lifetime. A weak hot-phonon effect is found at a low electric field. At higher electric fields, beyond the Ohm law, the hot-phonon lifetime plays a significant role. The drift velocity decreases with increasing hot-phonon lifetime for a given field value. Or the other way around, in order to reach a certain value of drift velocity, a much higher electric field has to be applied. In particular, the velocity of 6×10^6 cm s^{-1} (figure 4, thin green line) requires 2.4 times higher electric field when the lifetime is 3 ps (short dots) as compared with the result for 100 fs (dots). Short values of lifetime are preferable for switching applications since the desired value of current is supported at a lower consumed power.

The lifetime value of ~3 ps for plasmon-non-assisted hot-phonon conversion in GaN is not acceptable for the interpretation of the experimental data (figure 4, short-dot curve and closed stars). The model ignores elastic scattering mechanisms which are present, though weak. Therefore, the simulation results (curves) should exceed the experimental data (closed stars), but this is not the case if the field is strong and the lifetime is long. The hot-phonon lifetime should be shorter than 370 fs in the range of electric fields $E > 2$ kV cm^{-1} (closed stars and solid curve).

Another estimate of the hot-phonon lifetime can be obtained from the noise experiment and power balance. The power consumed by an average electron is obtained following equation (4), where the results of electron velocity (stars in figure 4 for sample A) are used. The power increases in proportion to squared electric field (Figure 5, line) within the Ohm law. A slower power increase is observed at higher electric fields. Because of lower mobility and drift velocity, the consumed power is lower in sample B (squares). After equation (6) the hot-phonon conversion decides the power dissipation. In the temperature approximation, the dissipated power is controlled by the difference of the equivalent hot-phonon temperature and that of the bath. The electron and hot-phonon temperatures can be obtained from the experimental data on the hot-electron noise temperature.

The thin curves in figure 6 illustrate the calculation within the simplified approach under assumption that the lifetime is independent of the power. Under the Ohm law ($P_c < 1$ nW/electron, figure 5), the experimental results on the hot-electron temperature (open stars and squares, figure 6) are in between the curves for the lifetime values of 0.5 ps and 0.3 ps. The best fit curve is drawn for 370 fs (red thin line). Thus, the measured noise temperature and the supplied power lead to estimation of the lifetime; the value $\tau_{LO} = 370$ fs suits the experimental data at low electric fields ($E < 2$ kV cm^{-1}, $P_c <$ 1 nW/electron).

The same value for the lifetime is not applicable at high power levels. Supposing the hot-phonon lifetime of 370 fs at supplied power of 30 nW/electron, the expected noise temperature would be ~1300 K (figure 6, thin red line) which is much too high compared to the experimental values (stars). A similar conclusion follows from the data on the drift velocity data (figure 4).

Let us estimate the effective occupancy of hot-phonon modes N_{LO} under the assumptions specified by equations (2)–(3). A linear dependence holds at low levels of supplied power $P_c < 1$ nW/electron (figure 7). However, the slope of the dependence decreases as the power increases. At high power levels, the bath temperature does not remain constant, but increases almost linear with supplied power (figure 6, dashed line). If the background occupancy N_b is subtracted, the experimental data on the excess occupancy $N_{LO} - N_b$ at $P_c > 10$ nW/electron (figure 7, closed triangles) can be fitted with a straight line and its slope yields the value of (32 ± 10) fs. Thus, the estimated value for the lifetime is (370 ± 100) fs at low level of supplied power and decreases rapidly as the power increases.

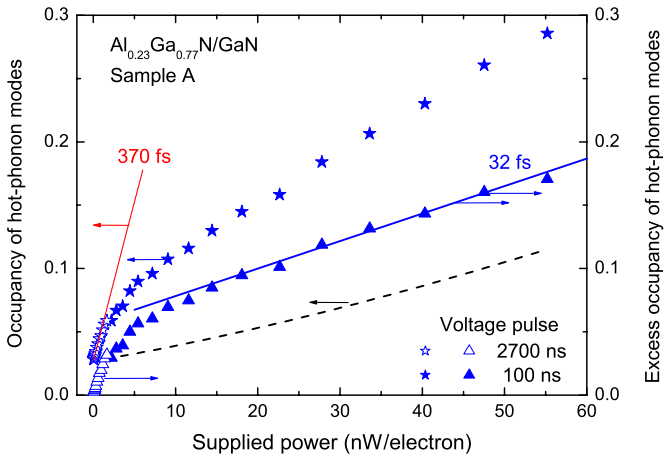

Figure 7. Power-dependent occupancy of LO-phonon states for passivated sample A: effective occupancy of hot-phonon modes N_{LO} (stars), background occupancy N_b (dashes), and excess occupancy $N_{LO} - N_b$ (triangles, right axis). Thin (red) and solid (blue) lines assume power-independent hot-phonon lifetime of 370 fs and 32 fs, respectively.

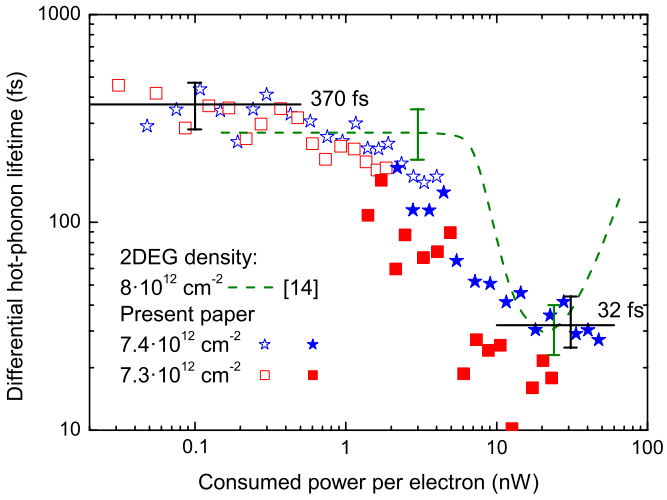

Figure 8. Differential hot-phonon lifetime for $Al_{0.23}Ga_{0.77}N$/GaN 2DEG channels: passivated sample A (stars) and unpassivated sample B (squares). Open symbols assume $T_b = T_0$, closed symbols take into account the power-dependent bath temperature (dashed line in figure 6). Dashed curve illustrates the experimental data for AlInN/AlN/GaN [14]. Black solid lines stand for 370 fs and 32 fs.

4. Discussion

The hot-phonon effects are considered in terms of different temperatures for the hot subsystem and the bath in the approach of hot-phonon lifetime. The validity of the assumptions has been thoroughly discussed elsewhere [4, 19]. The hot-phonon lifetime of $\tau_{LO} = (370 \pm 100)$ fs is extracted from the experimental data at low levels of power. This value is substantially lower than the plasmon-free lifetime for GaN (~2.5 ps [7, 10]); the plasmon-assisted conversion of hot phonons seems to be a plausible interpretation of the experimental data.

The plasmon–LO-phonon interaction becomes stronger when the frequencies of LO-phonons and plasma tend to match. The resonance takes place near 10^{19} cm^{-3} in bulk GaN. In order to estimate the electron density per unit volume in our samples, let us divide the 2DEG density, 7.4×10^{12} cm^{-2}, by the quantum well width at the Fermi energy, ~4 nm (figure 1). The obtained average density of $\sim 2 \times 10^{19}$ cm^{-3} exceeds that for the resonance conversion. The same conclusion follows from the comparison of the 2DEG density with the reported resonance density of $\sim 6.5 \times 10^{12}$ cm^{-2} for GaN-based 2DEG channels [12].

At elevated hot-electron temperatures, the bulk density decreases as the hot electrons occupy the upper subbands and the channel thickness increases [13]. The plasma frequency decreases together with decreasing bulk density. In other words, the resonance condition can be satisfied through electron heating at higher fields if the 2DEG density exceeds the resonance value at low electric fields. As mentioned, the approach of constant hot-phonon lifetime fails at high levels of supplied power (figure 6, thin lines and symbols). Let us discuss hot-phonon conversion in terms of plausible power-tunable resonance.

The power-dependent (differential) hot-phonon lifetime $\tilde{\tau}_{LO}$ can be introduced as follows [12]:

$$\tilde{\tau}_{LO} = \hbar\omega \frac{d(\Delta N_{LO})}{dP_c}. \quad (7)$$

Following equation (7), the differential hot-phonon lifetime can be estimated in a wide range of consumed power. Open symbols in figure 8 assume that the bath temperature is determined by the heat sink ($T_b = T_0$), closed symbols take into account the background occupancy of the LO-phonon modes (dashed curve in figure 7). The differential lifetime decreases as the power increases. The steepest decrease takes place at power $P_c \sim 2$ nW/electron ($E \sim 3$ kV cm^{-1}, $T_e \sim 400$ K). The results illustrate the power-tunable decay of hot phonons. Let us compare these results with those for AlInN/AlN/GaN channel [14].

Dashed line in figure 8 fits the experimental data for the AlInN/AlN/GaN channel with a similar 2DEG density [14]. The shape of the curve illustrates the power-tunable plasmon-assisted resonance. The lifetime decreases, reaches the minimum value of ~30 fs, and increases again as the power increases. The resonance condition is satisfied at ~20 nW/electron for the 2DEG channel located in the AlInN/AlN/GaN channel. Some similarities and distinction of the dashed curve with the data for sample A can be noted.

The 2DEG density of 7.4×10^{12} cm^{-2} for sample A (figure 8, stars) is close to that for the AlInN/AlN/GaN channel (8×10^{12} cm^{-2}). Correspondingly, the estimated low-power lifetime demonstrates close values. The resonance value (30 fs at ~20 nW/electron) is in reasonably good agreement with the high-power values for sample A .

On the other hand, the investigated $Al_{0.23}Ga_{0.77}N$/GaN samples demonstrate two important distinctions: the lifetime starts decreasing at considerably lower power, and no increase in the lifetime is observed at high power. A possible cause for the differences may originate from different electron density

profiles. While the AlN spacer keeps the 2DEG inside the GaN layer in the AlInN/AlN/GaN structure, the electron wave functions penetrate into the $Al_{0.23}Ga_{0.77}N$ barrier in the investigated structures (figure 1). The penetration becomes significant when the upper subbands are occupied due to high consumed power at elevated hot-electron temperatures. These distinctions are good for switching applications, since the lower values of lifetime support the desired current at a lower level of consumed power.

5. Summary

The hot-electron transport and heat dissipation are treated in terms of the temperatures different for the hot subsystem and the thermal bath. The hot-subsystem temperature is determined through measurement of the noise temperature at the microwave frequency. The observed increase in noise temperature at low levels of power is interpreted in the approach of constant hot-phonon lifetime: $\tau_{LO} = (370 \pm 100)$ fs. The experimental data on hot-electron drift velocity agree with those of Monte Carlo simulation within the model based on self-consistent solution of coupled Schrödinger–Poisson equations when the same value of the lifetime is used as an input parameter at low-moderate electric fields. This value of the lifetime is substantially lower than the plasmon-free lifetime. Moreover, the lifetime decreases as the power increases: the high-field value is below 50 fs. These are good news for switching applications, because the power-dependent lifetime means that the desired values of drift velocity and current can be obtained at lower electric field. The plasmon-assisted conversion of hot phonons is a plausible interpretation of the experimental data.

Acknowledgments

This research is funded by the European Social Fund under the Global Grant measure (grant N VP1-3.1-MM-07-K-03-038).

References

[1] Baliga B J 2013 Gallium nitride devices for power electronic applications *Semicond. Sci. Technol.* **28** 074011
[2] Su M, Chen Ch and Rajan S 2013 Prospects for the application of GaN power devices in hybrid electric vehicle drive systems *Semicond. Sci. Technol.* **28** 074012
[3] Kocevar P 1985 Hot phonon dynamics *Physica B&C* **134** 155
[4] Matulionis A, Liberis J, Matulionienė I, Ramonas M and Šermukšnis E 2010 Ultrafast removal of LO-mode heat from a GaN-based two-dimensional channel *Proc. IEEE* **98** 1118
[5] Matulionis A, Liberis J, Matulionienė I, Ramonas M, Eastman L F, Shealy J R, Tilak V and Vertiatchikh A 2003 Hot-phonon temperature and lifetime in a biased $Al_xGa_{1-x}N$/GaN channel estimated from noise analysis *Phys. Rev.* B **68** 035338
[6] Ridley B K 1996 The LO phonon lifetime in GaN *J. Phys.: Condens. Matter* **8** L511
[7] Tsen K T, Kiang J G, Ferry D K and Morkoç H 2006 Subpicosecond time-resolved Raman studies of LO phonons in GaN: dependence on photoexcited carrier density *Appl. Phys. Lett.* **89** 112111
[8] Kayis C, Ferreyra R A, Wu M, Li X, Özgür Ü, Matulionis A and Morkoç H 2011 Degradation in InAlN/AlN/GaN heterostructure field-effect transistors as monitored by low-frequency noise measurements: hot phonon effects *Appl. Phys. Lett.* **99** 063505
[9] Matulionis A, Liberis J, Šermukšnis E, Ardaravičius L, Šimukovič A, Kayis C, Zhu C Y, Ferreyra R, Avrutin V, Özgür Ü and Morkoç H 2012 Window for better reliability of nitride heterostructure field effect transistors *Microelectron. Reliab.* **52** 2149
[10] Dyson A and Ridley B K 2008 Phonon-plasmon coupled-mode lifetime in semiconductors *J. Appl. Phys.* **103** 114507
[11] Matulionis A 2009 GaN-based two-dimensional channels: hot-electron fluctuations and dissipation *J. Phys.: Condens. Matter* **21** 174203
[12] Matulionis A 2009 Ultrafast decay of non-equilibrium (hot) phonons in GaN-based 2DEG channels *Phys. Status Solidi (C) Conf.* **6** 2834
[13] Matulionis A, Liberis J, Matulionienė I, Šermukšnis E, Leach J H, Wu M and Morkoç H 2011 Novel fluctuation-based approach to optimization of frequency performance and degradation of nitride heterostructure field effect transistors *Phys. Status Solidi* A **208** 30
[14] Matulionis A, Liberis J, Matulionienė I, Ramonas M, Šermukšnis E, Leach J H, Wu M, Ni X, Li X and Morkoç H 2009 Plasmon-enhanced heat dissipation in GaN-based two-dimensional channels *Appl. Phys. Lett.* **95** 192102
[15] Šermukšnis E, Liberis J, Ramonas M, Matulionis A, Leach J H, Wu M, Avrutin V and Morkoç H 2011 Camelback channel for fast decay of LO phonons in GaN heterostructure field-effect transistor at high electron density *Appl. Phys. Lett.* **99** 043501
[16] Matulionis A 2013 Electron density window for best frequency performance, lowest phase noise and slowest degradation of GaN heterostructure field-effect transistors *Semicond. Sci. Technol.* **28** 074007
[17] Šimukovič A, Matulionis A, Liberis J, Šermukšnis E, Sakalas P, Zhang F, Leach J H, Avrutin V and Morkoç H 2013 Plasmon-controlled optimum gate bias for GaN heterostructure field-effect transistor *Semicond. Sci. Technol.* **28** 055008
[18] Ramonas M, Matulionis A, Liberis J, Eastman L F, Chen X and Sun Y J 2005 Hot-phonon effect on power dissipation in a biased $Al_xGa_{1-x}N$/AlN/ channel *Phys. Rev.* B **71** 075324
[19] Liberis J, Matulionienė I, Matulionis A, Ramonas M and Eastman L F 2009 Hot phonons in high-power microwave HEMT and FET channels *Advanced Semiconductor Materials and Devices Research—SiC and III-Nitrides* ed H-Y Cha (Kerala, India: Transworld Research Network) p 203–242